Synchrotron X-ray Reflectivity Study on the Structure of Templated Polyorganosilicate Thin Films and Their Derived Nanoporous Analogues

ARTICLE *in* LANGMUIR · SEPTEMBER 2001

Impact Factor: 4.46 · DOI: 10.1021/la010451c

3 AUTHORS, INCLUDING:

Joerg Bolze
PANalytical B.V.
21 PUBLICATIONS **675** CITATIONS

Synchrotron X-ray Reflectivity Study on the Structure of Templated Polyorganosilicate Thin Films and Their Derived Nanoporous Analogues

Jörg Bolze, Moonhor Ree,* and Hwa Shik Youn

Pohang University of Science & Technology, Department of Chemistry, Center for Integrated Molecular Systems and BK21 Functional Polymer Thin Film Group, and Pohang Accelerator Laboratory, San 31, Hyoja-dong, Pohang 790-784, South Korea

Sang-Hyon Chu and Kookheon Char

School of Chemical Engineering, Seoul National University, San 56-1, Shillim-dong, Kwanak-gu, Seoul 151-742, South Korea

Received March 26, 2001. In Final Form: August 3, 2001

Comprehensive X-ray reflectivity (XR) studies were conducted to characterize the structure of thin polyalkylsilicate films made of a poly(methylsilsesquioxane-*co*-ethylenylsilsesquioxane) precursor containing a star-shaped poly(ϵ-caprolactone) as a pore generator (porogen). The films were deposited on silicon wafer substrates by spin-coating and subsequently cured at various temperatures. Such spin-on glasses have a potential application as a low-dielectric-constant material for advanced semiconductors. Because high-intensity synchrotron X-ray radiation was used, the XR data could be measured over 9 orders of magnitude in intensity, which facilitated the observation of fine structural details. A hierarchical fitting procedure for modeling the XR data is given. By evaluation of the critical angle of total reflection of the film material, which was observed at smallest angles, in particular the film electron density could be determined with a high accuracy. The films cured at 420 °C show a lower electron density as compared to those cured at 250 °C. This is explained by the fact that at the higher temperature the porogen is calcined and escapes from the films leaving behind a nanoporous structure. Film porosities could be estimated from the observed changes in the electron densities. From the very large number of high-frequency oscillations observed in the XR curves, it is concluded that the films exhibit a homogeneous, well-defined structure with small interface and surface roughness. The film thickness could be determined with an accuracy of ±1 Å. The observation of an additional low-frequency modulation of the XR curves revealed a surface skin layer with a thickness of ca. 45 Å and with a slightly increased electron density as compared to the bulk of the film.

Introduction

Recently many research institutes and companies have been involved in the development of interlayer dielectrics with an ultralow dielectric constant *k* and a high dielectric strength. It is well conceived that by 2003 low-*k* material will be used in combination with copper interconnects in the back-end-of-the-line processes for the fabrication of integrated circuits with a feature dimension of 0.13 μm.[1] Indeed, IBM recently announced a semiconductor manufacturing process incorporating a low-*k* material for copper interconnects in the 0.13 μm process.[2,3] Continuous reduction of the dielectric constant to less than 2.2 seems to be inevitable for future generation devices and is believed to be only possible by incorporating nanometer-sized, air-filled pores in insulating matrixes.[4−6] One promising class of candidates for a low-*k* material is spin-on glasses, as, e.g., polyorganosilicate poly(methylsilsesquioxane) (PMSSQ), having an empirical formula of $(CH_3-SiO_{1.5})_n$.[7,8] It is characterized by an inherently low dielectric constant ranging from 2.7 to 2.9, a low moisture uptake, and an excellent thermal stability up to 500 °C.[6,9] Its dielectric constant may be further decreased when incorporating an organic supramolecular template as a pore generator (porogen) into the PMSSQ matrix and subsequently heating to elevated temperatures.[6,10,11] This results in the thermal decomposition and volatization of the porogen, leaving behind air-filled pores in the PMSSQ film. Star-shaped macromolecules such as poly(ϵ-caprolactone) as well as hyperbranched polyesters have proven to be suitable porogens.[7,11] Particularly in the case of high porosity, however, PMSSQ films have a potential lack of mechanical stability in various semiconductor fabrication steps such as chemical mechanical planarization and multilevel stacking. Reliable insulating thin films for chip integration are required to have a high surface hardness as well as mechanical toughness in order to withstand such severe mechanical stress conditions. In addition, the creation of closed pores in the matrix, which are not

* To whom correspondence should be addressed. Tel.: +82 54 279 2120. Fax: +82 54 279 3399. E-mail: ree@postech.edu.

(1) Chiang, S.-K.; Lassen, C. L. *Solid State Technol.* **1999**, *10*, 42.
(2) Carter, K. R. *Ultralow k Workshop*; ACS Division of Polymer Chemistry, Monterey, CA, Nov 14−17, 1999.
(3) Carter, K. R.; Dawson, D. J.; DiPietro, R. A.; Hawker, J.; Hedrick, J. L.; Miller, R. D.; Yoon, D. Y. U.S. Patent No. 5,895,263, April 20, 1999.
(4) Ree, M.; Goh, W. H.; Kim, Y. *Polym. Bull.* **1995**, *35*, 215.
(5) Hedrick, J. L.; Miller, R. D.; Hawker, C. J.; Carter, K. R.; Volksen, W.; Yoon, D. Y.; Trollsas, M. *Adv. Mater.* **1998**, *10*, 1049.
(6) Nguyen, C. V.; Carter, K. R.; Hawker, C. J.; Hedrick, J. L.; Jaffe, R. L.; Miller, R. D.; Remenar, J. F.; Rhee, H.-W.; Rice, P. M.; Toney, M. F.; Trollsas, M.; Yoon, D. Y. *Chem. Mater.* **1999**, *11*, 3080.
(7) Bagley, B. G.; Gallagher, P. K.; Quinn, W. E.; Amos, L. J. *Mater. Res. Symp. Proc.* **1984**, *32*, 287.
(8) Oh, W.; Shin, T. J.; Ree, M.; Jin, M. Y.; Char, K. Submitted for publication in *Chem. Mater.*
(9) Cook, R. F.; Liniger, E. G. *J. Electrochem. Soc.* **1999**, *146*, 4439.
(10) Ying, J. Y.; Mehnert, C. P.; Wong, M. S. *Angew. Chem., Int. Ed.* **1999**, *38*, 56.
(11) Nguyen, C. V.; Hawker, C. J.; Miller, R. D.; Huang, E., Hedrick, J. L.; Gauderon, R.; Hilborn, J. G. *Macromolecules* **2000**, *33*, 4281.

10.1021/la010451c CCC: $20.00
Published on Web 09/22/2001

interconnected, is an important requirement because pore interconnectivity would result in a low mechanical strength and in a low breakdown voltage. Recently Lee et al.[12] have shown that cured PMSSQ films which contain a small amount of an alkylene-bridged organosilicate (bis(1,2-trimethoxysilyl)ethane, BTMSE) as a comonomer exhibit better mechanical properties than PMSSQ homopolymer films and a better mixing with poly(ϵ-caprolactone).

Several on-wafer techniques have been applied to characterize the structure and properties of porous thin films. A recent review article by Morgen et al. nicely summarizes and explains these techniques as well as the results obtained by various research groups.[13] Specular X-ray reflectivity (XR) can give detailed structural information about thin films in terms of the laterally averaged electron density profile along the film surface normal.[14,15] Using XR, the electron density ρ_e of a thin film deposited on a substrate may be determined independently from the film thickness. This is a great advantage over optical methods, in which the determination of refractive index and thickness of a film cannot be done independently. As the electron density of the film is directly proportional to its mass density, a precise determination of this value is highly desirable for the characterization of the nanoporous thin films described above.

In most cases ρ_e (film) is deduced from XR data by a fit that may properly describe the fringes which usually appear in the decaying reflectivity curve if the film has a well-defined thickness and an electron density which is different from that of the substrate. These so-called Kiessig fringes[16] are explained by the interference of the X-ray beams which are reflected at the top surface and at the film−substrate interface, respectively. The amplitude of those fringes depends on the electron density difference between the film and the substrate. In many cases, ρ_e (substrate) is known a priori from the physical properties of the material (e.g., silicon wafer, glass, etc.) or it may be determined from a separate XR measurement of the bare substrate. Thus ρ_e (film) may be estimated. However, one has to bear in mind that the amplitude of the fringes is also strongly influenced by the roughness of the film interfaces, by possible large-scale film thickness nonuniformities, by the exact shape of the density profile at the interface,[17] by the instrumental resolution, or by a possible curvature of the substrate. Furthermore, radiation damage of the film material may result in a partial smearing of the fringes. Due to this, the uncertainties and errors in the determination of ρ_e (film) by this procedure may become quite significant and in the case of very rough layers it becomes virtually impossible. In many cases there exists an alternative, highly accurate method to determine ρ_e (film): if ρ_e(film) < ρ_e(substrate), one may observe two critical angles of total X-ray reflection, the smaller one being associated with the film material and the larger one with the substrate.[14,15] As the position of the critical angle of the film is directly related to ρ_e(film) (see below) and independent of the above-mentioned parameters, the determination of ρ_e(film) becomes much more straightforward. This is a very elegant and precise method to determine the density of thin layers, which surprisingly has not been applied frequently for that purpose. Only very recently have some papers appeared which nicely demonstrated the practical value of this method to determine the electron density of a thin nanoporous layer, which may be either an integral part of the substrate[18,19] or where a film is attached to a substrate and cannot be removed due to its fragility.[20] As the critical angle of the film appears at very small angles (a few tenths of a degree at most), a well-collimated X-ray beam with a small angular divergence is essential to successfully apply this method. Here synchrotron X-ray radiation is particularly useful due to its naturally low divergence. In addition great care in a very precise sample alignment is necessary, because any uncertainty in the position of the critical angle directly translates in an uncertainty in the determination of ρ_e(film).

In this study, we have used X-ray reflectivity to characterize the structure of thin poly(methylsilsesquioxane-*co*-ethylenylsilsesquioxane) (in the following abbreviated as "PMSSQ/BTMSE") copolymer films containing various initial amounts of a porogen. The porogen used was a star-shaped poly(ϵ-caprolactone). Curing temperatures were chosen below and above the decomposition temperature of the porogen. A particular interest in this work was a highly precise electron density determination of these thin films in order to study the effectiveness of the porogen as a pore generator. For this purpose, any changes in the critical angle corresponding to the film material were monitored and evaluated. To date, the few XR works on poly(silsesquioxane) films which were reported[20,21] provide data only in a rather limited range of intensities, typically over 3−5 orders of magnitude. Here we used high-intensity synchrotron X-ray radiation in order to measure XR data to reflectivities as low as possible, for revealing any possible inhomogeneities within the film with a good resolution. A hierarchical fitting procedure for extracting structural information is given and the possibilities and limitations of this experimental method for characterizing nanoporous thin films are critically discussed.

Experimental Section

Preparation of the Prepolymer and Porogen. The PMSSQ/BTMSE prepolymer was prepared by a similar synthetic procedure as described by Takamura et al.[22] for the case of PMSSQ. Bis(1,2-trimethoxysilyl)ethane (BTMSE) was added to methyltrimethoxysilane (MSSQ) as a comonomer by 10 mol %, followed by a sol−gel reaction. The number- and weight-average molecular weights of the copolymerized prepolymer were $\overline{M}_n$ = 2700 g/mol and $\overline{M}_w$ = 5200 g/mol. A star-shaped poly(ϵ-caprolactone) (PCL), which bears a biphenyl core and four polyester arms with hydroxyl end groups (Chart 1), was synthesized according to a procedure described elsewhere,[23,24] leading to $\overline{M}_n$= 4390 g/mol and $\overline{M}_w$ = 5180 g/mol and a degree of polymerization (DP) of 7.3/arm. All molecular weights were measured by gel permeation chromatography based on polystyrene standards. A thermogravimetric analysis (TGA) of the PCL itself has shown, that a major decomposition and volatization of the PCL

(12) Lee, J. K.; Char, K.; Chu, S. H.; Yoon, D. Y. Submitted for publication in *Chem. Mater.*

(13) Morgen, M.; Ryan, E. T.; Zhao, J.-H.; Hu, C.; Cho, T.; Ho, P. S. *Annu. Rev. Mater. Sci.* **2000**, *30*, 645 and further references given therein.

(14) Tolan, M. *X-ray scattering from soft matter thin films*; Springer-Verlag: Berlin, Heidelberg, 1999.

(15) Holy, V.; Pietsch, U.; Baumbach, T. *High-resolution X-ray scattering from thin films and multilayers*; Springer-Verlag: Berlin, Heidelberg, 1999.

(16) Kiessig, H. *Ann. Phys.* **1931**, *10*, 769.

(17) You, H.; Melendres, C. A.; Nagy, Z.; Maroni, V. A.; Yun, W.; Yonco, R. M. *Phys. Rev. B* **1992**, *45*, 11288.

(18) Buttard, D.; Dolino, G.; Bellet, D.; Baumbach, T.; Rieutord, F. *Solid State Commun.* **1999**, *109*, 1.

(19) Chamard, V.; Dolino, G.; Stettner, J. *Physica B* **2000**, *283*, 135.

(20) Wu, W.; Wallace, W. E.; Lin, E. K.; Lynn, G. W.; Glinka, C. J.; Ryan, E. T.; Ho, H. M. *J. Appl. Phys.* **2000**, *87*, 1193.

(21) Wu, W.; Liou, H.-C. *Thin Solid Films* **1999**, *312*, 73.

(22) Takamura, N.; Gunji, T.; Hatano, H.; Abe, Y. J. *J. Polym. Sci., Part A: Polym. Chem.* **1999**, *37*, 1017.

(23) Trollsas, M.; Hedrick, J. L.; Mecerreyes, D.; Dubois, Ph.; Jerome, R.; Ihre, H.; Hult, A. *Macromolecules* **1997**, *30*, 8508.

(24) Trollsas, M.; Hedrick, J. L. *J. Am. Chem. Soc.* **1897**, *19*, 4644.

Chart 1. Chemical Structure of the Star-Shaped Four-Arm Poly(ϵ-caprolactone) (PCL) Which Was Used as a Porogen (DP/arm = 7.3)

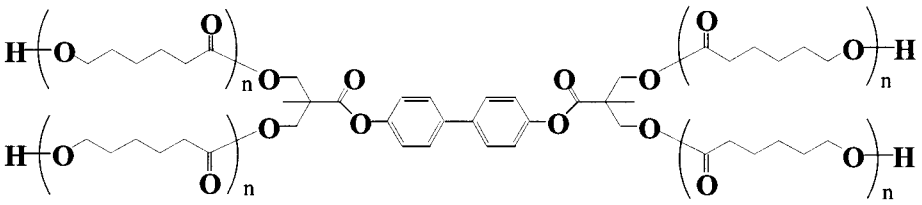

starts at a temperature around 260 °C. At 420 °C less than 5% of the original weight of the PCL is remaining.

Film Preparation. Si(100) wafers were cut into pieces of ca. 45 × 30 mm^2 and cleaned with piranha solution, followed by rinsing with deionized water and drying in a nitrogen stream. The PMSSQ/BTMSE prepolymer and PCL were dissolved and mixed in methyl isobutyl ketone with a total solid content of 20 wt %. PCL contents were adjusted to 0, 10, and 20 wt % with respect to the total solid content. The homogeneous mixtures were deposited on the silicon wafers using a disposable syringe equipped with an 0.2-μm PTFE microfilter. Smooth films were prepared by spin-coating at 5000 rpm for 30 s. The deposited films were heated under vacuum at 2 °C/min up to 100 °C and held at that temperature for 1 h. They were then further heated to 250 °C and cured at that temperature for one additional hour before slowly cooling. During this curing process the matrix material vitrifies via a bulk polymerization process and one yields the matrix/porogen hybrid system. For obtaining porous films, another set of samples was prepared in exactly the same way as described above, but the curing temperature was further increased from 250 to 420 °C and held at that temperature for 1 h before cooling down. At that higher temperature a full curing of the matrix is going on. In addition the thermal decomposition (calcination) of the porogen and a resulting mesporous film structure are expected. The thicknesses of all films were ca. 100 nm.

X-ray Reflectivity. X-ray reflectivity data were measured using synchrotron radiation at the bending magnet X-ray diffraction beamline BL3C2[25] of the Pohang Light Source in Korea. By use of a Si(111) double crystal monochromator, a wavelength, λ, of 0.154 nm was selected with $\Delta\lambda/\lambda = 5 \times 10^{-4}$. X-rays were focused onto the sample by a toroidal, platinum-coated silicon mirror. The sample was mounted on a HUBER four-circle goniometer, and a scintillation counter with an enhanced dynamic range (Bede Scientific, EDR) was used as a detector. The beam size was defined by a slit, S1, located 153 cm before the sample. Another slit, S2 (placed 80 cm behind S1), was used to cut the tails of the beam (due to the slit scattering of S1) without affecting the intensity of the main beam. An antiscattering slit, S3 (37 cm behind the sample), effectively cut down the scattering from sources other than the sample. The detector slit, S4, was placed 74 cm behind the sample. The horizontal beam size at the sample position was ca. 2 mm, and the full width at half-maximum of the direct beam profile measured by a detector scan was 0.015°.

The measured reflected intensities were normalized to the intensity of the primary beam, which was monitored by an ionization chamber. Specular reflection was measured by scanning the tilt angle θ of the sample surface with respect to the primary beam direction and by simultaneously moving the detector arm by 2θ. Reflectivities, R, i.e., the ratio of the intensities of the reflected and incident beam intensities, could thus be measured down to 10^{-9}. To cover such a wide dynamic range, aluminum attenuators of various thicknesses were inserted into the beam where the reflected intensities exceeded the saturation level of the detector. For an accurate determination of the critical angles of the silicon wafer and of the thin film, θ was scanned at the smallest possible increments (0.001°) at angles smaller than 0.8°. At higher angles it was sufficient to increase the step width to 0.002−0.005°. At reflectivities below ca. 10^{-8}, diffuse scattering due to surface and interface roughness (scattered "by chance" in the specular direction) as well as parasitic scattering

(25) Park, B.-J.; Rah, S.-Y.; Park, Y.-J.; Lee, K.-B. *Rev. Sci. Instrum.* **1995**, *66*, 1722.

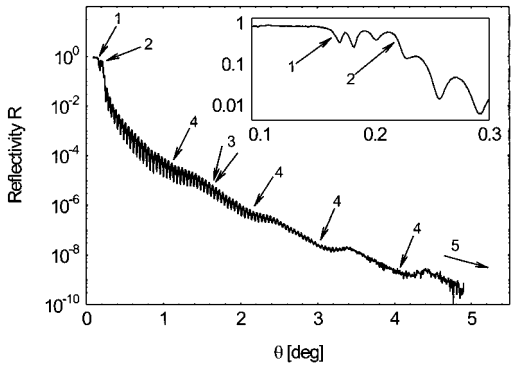

Figure 1. A representative X-ray reflectivity curve measured from one of the thin polyorganosilicate films (PMSSQ/BTMSE copolymer matrix which originally contained 10 wt % of porogen, cured at 420 °C). A number of characteristic features are evident: a critical angle of the film material (1); a critical angle of the silicon substrate (2); a large number of very regular, high-frequency oscillations (3); a low-frequency modulation with a small amplitude (4); a certain decay of the whole curve (5). Note that the decay of the reflected intensity could be measured over 9 orders of magnitude. The inset shows a magnification of the region around the two critical angles.

from the optical components became significant. These contributions were measured separately by additional scans, where the detector was moved by a constant offset of $\delta = 0.04°$ with respect to the specular angle 2θ. The intensities measured in such $[\theta - (2\theta + \delta)]$ and $[\theta - (2\theta - \delta)]$ scans were averaged and subtracted from the intensities measured in a $(\theta - 2\theta)$ scan. This background for the reflectivity scans did not exceed 10% of the reflectivity itself over the angular range of the measurements. A total of about 4 h was necessary to record a complete set of specular and offset scans for one sample.

Special care was taken for a precise sample alignment, which was done as follows: First the origin of 2θ was determined from the angular position of the maximum intensity measured in a 2θ scan of the detector through the direct beam. The origin of 2θ was reconfirmed before and after the measurement of each sample. The sample height was adjusted by an iterative procedure of vertical movement and rocking of the sample across the primary beam until the maximum intensity of a rocking scan equals half of the intensity of the full primary beam. To determine the origin of θ, the detector was scanned through the specular reflected beam while keeping the incident angle at a constant value. θ was properly rescaled so that the maximum in the 2-Å detector scan equals two times the incident angle. For highest precision, this procedure was repeated at various incident angles. In this way, the sample could be aligned with a precision of ca. ±0.001°.

Results and Discussion

A typical reflectivity curve as measured from the polyorganosilicate films over 9 orders of magnitude in the intensity is shown in Figure 1.

In the following we will discuss some characteristic features which are present in all measured XR curves and which may be used to extract structural information. At grazing incident angles θ smaller than a certain critical angle θ_c(film) (feature 1), the beam is totally reflected

from the film surface and the reflectivity R is essentially 1. Here the beam does not penetrate into the film and there is only an evanescent wave traveling through the film surface. Once the incident angle exceeds the critical angle of the film, a portion of the beam is also transmitted through the film and totally reflected at the interface between the film and the substrate as long as $\theta_c(\text{film}) < \theta < \theta_c(\text{substrate})$. Here the beam still does not penetrate into the substrate. The oscillations between the two critical angles (feature 1) and (feature 2) are the waveguide modes for X-rays confined in the film. Thus, the reflected intensity is close to the incident one. Due to a certain degree of absorption of X-rays in the film, however, the intensity is slightly decreased. Actually the existence of a critical angle of the film is an absorption effect; in the case of zero absorption, one would observe a reflectivity of unity for all angles smaller than the critical angle of the substrate. Furthermore, two critical angles are only observed if the electron density of the film is smaller than that of the substrate, as it is the case here.

The inset shows that two critical angles, which are attributed to the film (feature 1) and the substrate (feature 2), respectively, could be clearly observed in the experimental data. The critical angle is directly related to the average electron density ρ_e of the corresponding material by[14]

$$\theta_c = \lambda\,(\rho_e r_e/\pi)^{1/2} \qquad (1)$$

where λ represents the wavelength of radiation and r_e is the classical electron radius. Note that the position of the critical angle of the film only depends on the average film electron density and not on the exact electron density distribution within the film. Thus the average electron densities of the film and the substrate are directly determined by the two critical angles, and they can be transformed into mass densities if the chemical compositions of the materials are known. The electron density is directly proportional to the mass density. Indeed, X-ray reflectivity is a very powerful and unique tool for precise measurements of the densities of very thin films, which is hardly possible with any other experimental method.[15,20] The precision in the determination of the critical angle of $\pm 0.001°$ as achieved in our experiments corresponds to an accuracy in the deduced value of the film electron density of $\pm 1.2\%$.

Once θ exceeds the critical angle of the substrate, a significant portion of the beam also penetrates into the substrate and a sharp dropoff of the reflected intensity occurs. The steeply decaying reflectivity curve is modulated by several high-frequency oscillations (feature 3), which are commonly referred to as Kiessig fringes.[16] These fringes appear due to the interference of the beams reflected from the film surface and from the film/substrate interface, respectively. It can be shown, that for a film of thickness d, the angular maximum position $\theta_{m,max}$ of the Kiessig fringe of order m is given by eq 2.

$$\sin^2(\theta_{m,\max}) = m^2(\lambda/2d)^2 + \sin^2(\theta_c(\text{film})) \qquad (2)$$

This equation may be seen as a converted form of the well-known Bragg equation, modified by the influence of refraction in the film. Thus, when the experimental data are plotted according to eq 2, the total film thickness can be determined from the slope of the straight line which fits the data points (Figure 2). It can be seen, that all data points are very well described by the linear fit. As we could observe more than 70 highly regular Kiessig fringes, the total film thickness may be determined very accurately from Figure 2 to 999 ± 1 Å. Furthermore, it can be concluded that a well-defined film structure is present.

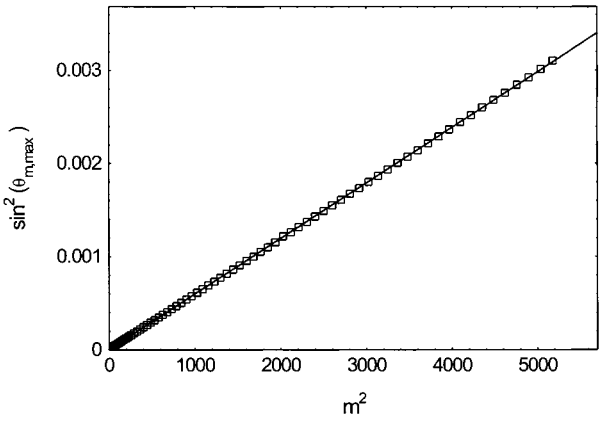

Figure 2. Plot of the experimental data (□) displayed in Figure 1 according to the modified Bragg equation given in eq 2. The solid line represents a linear fit. From the slope of the fit curve, the film thickness can be determined very accurately to 999 ± 1 Å.

According to eq 2, θ_c(film) could principally be determined from the intersection point of the linear fit curve with the ordinate in Figure 2. If the critical angle is to be determined in that way, however, for better accuracy one is advised to take into account the first few fringe maxima only. In addition to the high-frequency modulation (feature 3) of the curve in Figure 1, another modulation (feature 4) with a considerably lower frequency could be observed in all measured curves. This indicates the presence of a thin layer ($d = 43$ Å) in addition to the bulk of the film ($d = 956$ Å). The origin of this thin layer will be discussed further below. With increasing angle the curves show a certain overall decay of the reflected intensity and of the modulation amplitudes (feature 5). According to the Fresnel law the reflectivity is proportional to the inverse fourth power of the scattering angle at $\theta \gg \theta_c$. Due to interface and surface roughness, this decrease is further enhanced by additional exponential damping factors. Thus, by measuring the reflectivity curve in a wide dynamic range up to highest possible angles, detailed information about surface and interface roughness becomes available.

Before fitting a model electron density profile to the experimental data, it was necessary to correct the raw data for a geometrical effect: at very small angles, the size of the beam projected onto the sample surface plane was larger than the sample which results in a distortion of the reflectivity curve; as the incident angle increases, the portion of the direct beam which is reflected by the sample surface increases steadily, which is evident in the positive slope of the measured intensity shown in Figure 3. Following a procedure given by Gibaud et al.[26] an angle-dependent correction factor for the intensity was used to compensate this distortion effect at smallest angles. In the first approximation a uniform incident beam of rectangular shape was assumed which results in a correction factor of (constant/sin(θ)). The main effect of this correction procedure is a change in the slope of the reflectivity curve in that angular region and in the height of the overall curve. On the other hand, it does not affect the positions of the two critical angles or of the maxima and minima in the Kiessig fringes. This is also true for the more realistic case of a Gaussian direct beam profile.

(26) Gibaud, A.; Vignaud, G.; Sinha, S. K. *Acta Crystallogr.* **1993**, *A49*, 642.

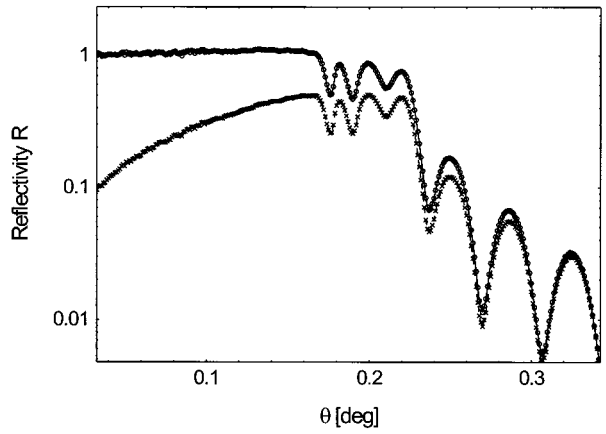

Figure 3. Distortion of the experimental data (×) due to the fact that at smallest angles the beam size projected onto the sample surface plane is larger than the sample itself. By use of an angle-dependent correction factor, this distortion effect could be compensated. The corrected curves (○) show a reasonably flat plateau region of total reflection at angles smaller than the critical angle of the film.

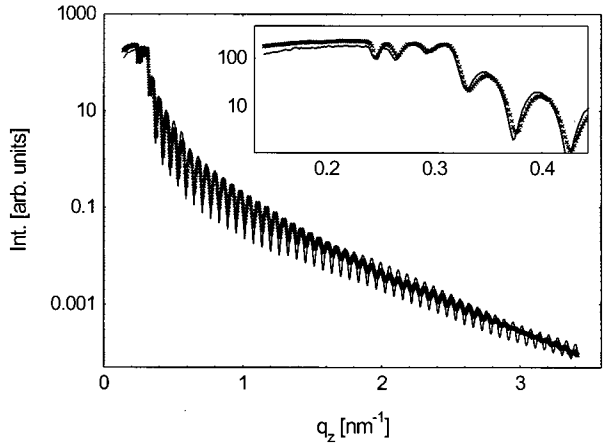

Figure 4. Effect of a prolonged exposure of the thin PMSSQ/BTMSE copolymer films to synchrotron X-ray radiation: solid line, first measurement; marks, repeated scan after ca. 4 h of irradiation. The inset shows a magnification of the region between the two critical angles. A considerable smearing of the deep minima of the Kiessig fringes is evident. On the other hand, the overall decay of the curve and in particular the positions of the critical angles are hardly affected.

So principally it is possible to extract the correct critical angles from the raw data already. As demonstrated in Figure 3, the curves corrected in this way show a reasonably flat plateau region of total external reflection at angles smaller than the critical angle of the film.

Despite minimizing the X-ray exposure time of the samples, some effects of radiation damage were apparent. After the completion of a measurement, in some cases a weak spot was visible on the sample surface on the area which was hit by the X-ray beam. So we have carefully checked the reproducibility of the experimental data. As shown in Figure 4, repeated scans typically resulted in a considerable smearing of the deep minima in the Kiessig fringes. On the other hand, the overall decay of the curve and in particular the positions of the critical angles were hardly affected. This distortion gives some uncertainty in the roughness parameters of the various interfaces. However, the average film electron density, which was determined from the position of the critical angle, is a very reliable value. In that angular range, which was scanned first, the number of photons per unit sample area is relatively small because the incident beam is spread over a very large sample area and because in addition attenuators were inserted into the beam. Radiation damage is more likely to affect the data at intermediate and higher angles, where the projected beam size is small, where all attenuators were removed and exposure times per data point were relatively long. This is also supported by the data displayed in Figure 4.

Evaluation of the X-ray reflectivity profiles was done by a least-squares fitting procedure of parametrized model electron density profiles to the experimental data. Calculations were done with a recursive formula given by the dynamical theory of Parratt,[27] which properly incorporates absorption, refraction, as well as multiple scattering effects. Interfacial roughness was taken into account by introducing Névot−Croce damping factors into the recursive formula, assuming Gaussian smearing functions.[28] In the following, specular reflectivities will be discussed as a function of the magnitude of the scattering vector $\vec{q}$, which is related to the incident angle θ by

$$|\vec{q}| = |\vec{q}_z| = \frac{4\pi}{\lambda}\sin(\theta) \tag{3}$$

Note that in the case of specular reflection, $\vec{q}$ is oriented strictly perpendicular to the sample surface. This means that one probes the electron density profile along the sample surface normal (z-direction) while laterally averaging over a sample area which corresponds to the projected coherence length of the incident X-rays. The electron density profile is modeled as a stack of slabs with a constant electron density in each slab. Each slab is characterized by its thickness d, by the root-mean-square width σ of the Gaussian smearing functions at the adjacent interfaces, and by the complex refractive index n. The latter incorporates both the electron density ρ and the linear attenuation coefficient μ for X-rays and is given as[27]

$$n = 1 - \delta + i\beta \tag{4}$$

where

$$\delta = \frac{1}{2\pi} r_e \lambda^2 \rho_e \tag{5}$$

and

$$\beta = \frac{\lambda}{4\pi}\mu \tag{6}$$

From the measured reflectivity curves as displayed in Figure 1, structural parameters were extracted in a hierarchical way with the following sequence: (i) The structural parameters of the silicon wafer were determined in a separate measurement of the bare wafer. (ii) The overall film thickness was precisely determined from a plot according to eq 2, as already demonstrated in Figure 2. (iii) The average electron density of the film was determined by fitting the measured data in the region around the two critical angles of the film and the substrate. As can be easily seen from eq 2, due to the refraction effect, the positions of the extrema in the oscillations in that angular range are very sensitive to the film electron density. (On the other hand, the extrema positions are basically independent from ρ_e(film) at intermediate and higher angles.) Thus, for best accuracy, one is advised to determine ρ_e(film) not just from the apparent measured

(27) Parratt, L. G. *Phys. Rev.* **1954**, *95*, 359.
(28) Névot, L.; Groce, P. *Rev. Phys. Appl.* **1980**, *15*, 761.

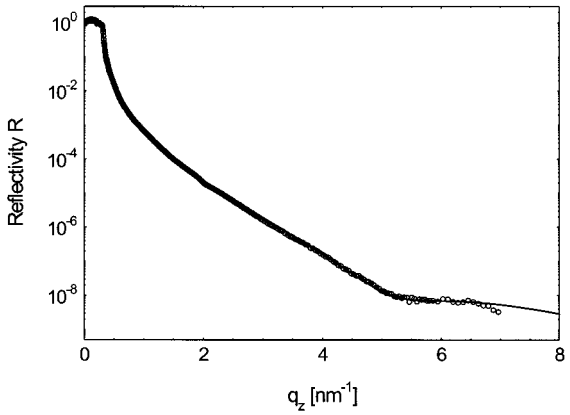

Figure 5. Measured reflectivity data (marks) from the bare silicon wafer and fit curve (solid line). The minimum observed at $q_z = 5.4$ nm^{-1} indicates the existence of a very thin, native silicon oxide layer with a thickness of 7 Å.

angle position of the first critical angle but from a fit which in particular best matches the first few extrema of the oscillations. In fact, for rather thin films ($d \approx 100$ nm) as considered here, the determination of the film electron density from the angle position of the first dip in the reflectivity profile would lead to an erroneous result, which exceeds the true value by as much as 5%. Only for films with a thickness of a few hundred nanometers and more, the angle position of the first dip correctly represents the real critical angle of the film. (iv) The imaginary part β of the refractive index of the film (cf. eq 6) was then determined from the height of the intensity level between the two critical angles, where absorption effects are most significant. (v) To take into account the low-frequency modulation (see feature 4 in Figure 1) of the reflectivity profile, an additional thin layer was added to the model, without changing the already determined total thickness and average electron density of the film. From the phase of the oscillations, it was unambiguously determined whether the electron density of this layer is higher or lower with respect to the bulk of the film. (vi) Finally, surface and interface roughness parameters were fitted so as to best match the overall decay of the reflectivity curve as well as the decay in the oscillation amplitudes of the Kiessig fringes.

Figure 5 displays the reflectivity curve measured from the bare silicon wafer which was used as a substrate. The curve shows a steady decay of the intensity over 8 orders of magnitude until a shallow minimum is reached at $q_z = 5.4$ nm^{-1}. This indicates the existence of a very thin, native silicon oxide layer. The minimum appears at the angle where the beams reflected at the top surface and at the Si/SiOx interface interfere destructively. It corresponds to an oxide layer thickness of only 7 Å. Note that this feature could only be observed because a high-intensity X-ray beam was available and due to a careful background subtraction. The critical angle of silicon appeared at 0.221° (critical scattering vector $q_c = 0.315$ nm^{-1}), which corresponds to a mass density of 2.3 g/cm^3, in good agreement with tabulated values. The fitted curve, which is also shown in Figure 5, describes the experimental data very well. The resulting fit parameters are as follows: d(SiOx) = 7 Å, δ(Si) = 7.447 × 10^{-6}, δ(SiOx) = 6.292 × 10^{-6}, β(Si) = 1.796 × 10^{-6}, β(SiOx) = 1.025 × 10^{-7}, σ(Si/SiOx) = 1.0 Å, and σ(SiOx/air) = 3.2 Å. It is concluded that the substrates have a very smooth surface. When fitting the XR data from the thin polyorganosilicate films, for all samples only minor deviations from these structural parameters of the substrate were allowed.

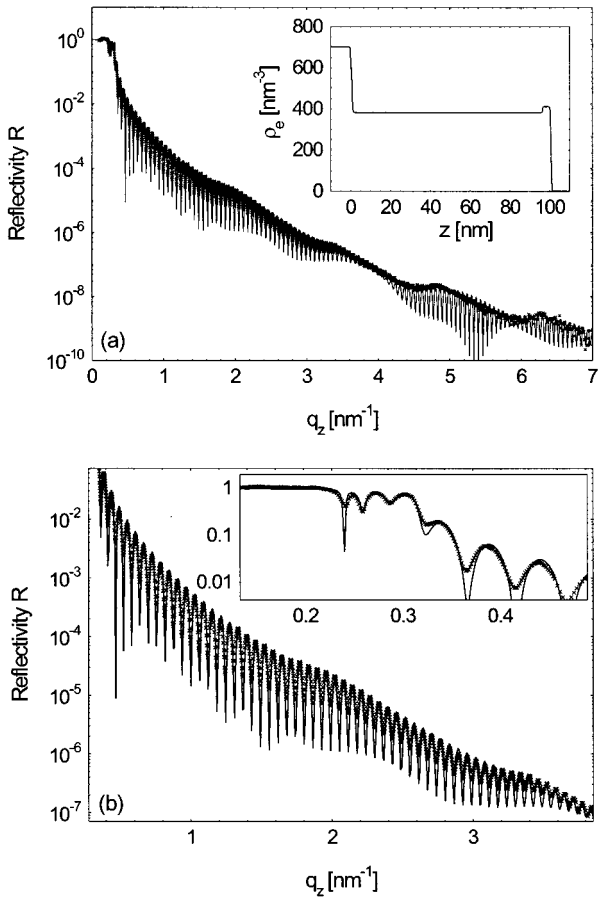

Figure 6. Measured reflectivity curve (marks) of the PMSSQ/BTMSE copolymer film which originally contained 10 wt % of porogen and which was cured at 420 °C (same curve as shown in Figure 1). The solid line represents the fit curve assuming a homogeneous electron density distribution within the film except for a thin surface skin layer, in which the electron density is slightly increased. The average film electron density was determined to 384 ± 5 nm^{-3} and the total film thickness to 999 ±1 Å. Part a shows the curves in the entire angular range where experimental data were collected together with the fitted electron density profile (inset). To demonstrate the quality of the fit more clearly, part b shows magnifications of the middle part of these curves as well as of the region around the two critical angles (inset).

Following the hierarchical fitting procedure as explained above, structural information about the polyorganosilicate films was extracted from the experimental data. As a representative example, Figure 6 displays the reflectivity curve of the film which originally contained 10 wt % of porogen and which was cured at 420 °C (the same curve as already shown in Figure 1). Also displayed are the fit curve and the corresponding electron density profile.

From a fit of the positions of the maxima and minima in the oscillations around the two critical angles (cf. inset of Figure 6b) the average electron density of the film could be precisely determined to 384 ± 5 nm^{-3}. Furthermore, the Kiessig fringes are very well matched at all angles by the fit with a total film thickness of 999 ± 1 Å as determined from Figure 2. The experimental data are well described with a model (see inset of Figure 6a), which assumes a homogeneous electron density distribution throughout the film except for a thin surface skin layer which has a thickness of ca. 43 Å and an electron density which is slightly increased by ca. 7% as compared to the bulk of the film. The presence of this skin layer results in the low-frequency modulation of the whole XR curve, and the phase of this modulation unambiguously indicates that the

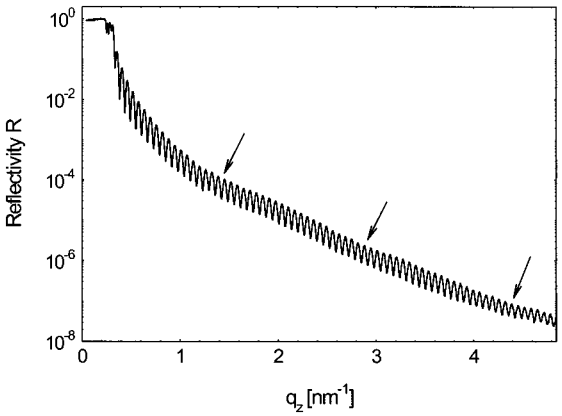

Figure 7. XR data of the PMSSQ/BTMSE copolymer film which was prepared without adding any porogen. The curing temperature was 250 °C. Here also, as in the case of the corresponding porogen-containing films, a low-frequency modulation of the XR curve (indicated by arrows) was observed.

electron density of the skin layer is higher than that of the underlying bulk of the film. The film surface roughness as determined from the decay of the XR curve amounts to 4.2 Å only, which indicates a very smooth surface. All features of the experimental data are well matched by the fit curve, except for the depth of the minima, which are considerably shallower in the experimental data. Assuming a higher electron density of the film (close to that of silicon oxide) would result in shallower minima in the model curve. However, the average film electron density is unambiguously fixed to 384 ± 5 nm^{-3} from the oscillations around the critical angles, and the above-mentioned assumption can thus be clearly ruled out. Assuming a considerably higher surface roughness would also result in shallower minima, but at the same time the overall decay of the curve would be much steeper than that observed. So this possibility may also be ruled out. A slightly inhomogeneous film thickness on the length scale of the projected beam size, however, would smear the oscillations to some degree due to the incoherent superposition of the intensities reflected at different positions across the wafer which correspond to different film thicknesses. A slight gradient of the film thickness from the center of the wafer toward the edges is certainly plausible for films prepared by spin coating. Furthermore, residual stress measurements performed in our lab[8] have shown that the coated silicon wafer is slightly bent due to thermal stress in the film. A curvature of the substrate also results in a smearing of the Kiessig fringes in XR data. Yet another explanation for the rather shallow minima in the experimental data seems to be the effect of radiation damage. Indeed, as already demonstrated in Figure 4, radiation damage was mainly evidenced by a smearing of the deep minima of the Kiessig fringes. As the other features of the XR curve (in particular the critical angle of the film) were not affected by radiation damage, it may be regarded as a minor problem. All the other films that we measured showed qualitatively the same characteristics as the data displayed in Figure 6. The low-frequency modulation was always observed, which indicates that a thin surface skin layer with a thickness of ca. 45 Å exists in all cases, irrespective of curing temperature and irrespective of porogen content (cf. Figure 7). Furthermore, the film surface roughness was determined to 4−5 Å in all cases. Thus, all data could be well fitted based on the type of electron density profile shown in the inset of Figure 6a.

Figure 8 displays for each sample the XR profiles around the critical angles together with the fitted curve. All fits

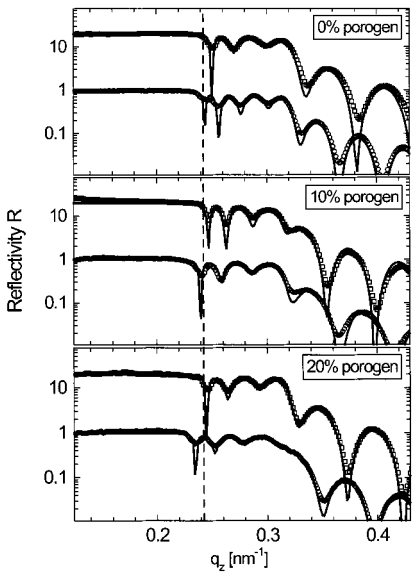

Figure 8. Experimental data around the two critical angles obtained from the films cured at 250 °C (□) and 420 °C (○) with initial porogen contents of 0 vol % (top), 10 vol % (middle), and 20 vol % (bottom). The solid lines represent the respective fit curves. For sake of clarity the curves corresponding to the samples cured at 250 °C were multiplied by a factor of 20, respectively. The dashed line is a reference to indicate the position of the critical angle of the film which did not contain any porogen and which was cured at 420 °C. With increasing porogen content and at the higher curing temperature, the critical angle of the film shifts to smaller values, indicating a decrease of the average film electron density.

Table 1. Fitted Thicknesses *d* and Electron Densities ρ_e of the Bulk Film Material and of the Skin Layer as a Function of the Initial Porogen Content and of the Curing Temperature[a]

porogen (wt %)	curing temp (°C)	*d*(bulk) (Å)	*d*(skin) (Å)	ρ_e(bulk) (nm^{-3})	ρ_e(skin) (nm^{-3})	$\rho_{e,av}$(film)[b] (nm^{-3})
0	250	914	45	418	440	419
0	420	1203	45	404	425	405
10	250	1044	44	411	446	412
10	420	956	43	383	411	384
20	250	940	43	401	436	403
20	420	1020	43	369	404	370

[a] The corresponding fit curves are displayed in Figure 8. [b] $\rho_{e,av}$ represents the average electron density of the polyorganosilicate film. The uncertainties for $\rho_{e,av}$ and for the total film thickness are ±5 nm^{-3} and ±1 Å, respectively. The complex part of the refractive index of the films was estimated to β(film) = $3.4 \times 10^{-8} \pm 4 \times 10^{-9}$ and surface roughness to 4−5 Å.

match well the maxima and minima of the experimental data and allow a precise determination of the respective average film electron densities. The fit parameters are summarized in Table 1. Comparing the average film electron densities of the samples cured at 250 °C, a slight decrease was observed with increasing porogen content. This shows that the electron density of the porogen is slightly smaller than that of the PMSSQ/BTMSE matrix material. In addition, this difference could be due to the decomposition of a small amount of the porogen already after curing at 250 °C. Furthermore, for each porogen content, the film electron density is lower for the samples cured at 420 °C as compared to those cured at 250 °C. This is directly evident from the shift of the critical angle of the film to smaller values when the curing temperature is higher. The difference in the electron densities between films cured at 250 and 420 °C is highest for the films which originally contained 20 wt % of porogen and it is smallest for the films which did not contain any porogen.

It is well-known, that when increasing the curing temperature from 250 to 420 °C, a vitrification process of the PMSSQ matrix is still going on in the form of intermolecular chain extension and cross-linking reactions, which is accompanied by a change of the mass density and of the chemical composition of the film.[6] The electron density depends on both of these parameters. As we did not determine the chemical composition of the film, we cannot infer its mass density from the electron density. Suffice it to say that the small change in electron density observed for the matrix material itself (Figure 8, top) reflects this vitrification process. The electron density of PMSSQ (ca. 400 nm^{-3}) is considerably lower than that of SiO_2 (ca. 700 nm^{-3}). This may be explained mainly with the presence of pendant, nonbinding methyl groups and of branched, ladder, as well as polyhedral, cagelike structures[29−31] in PMSSQ, which lead to a reduced mass density. Bagley et al. have shown by infrared spectroscopic measurements, that the methyl groups are not removed upon curing at 420 °C or below.[7] The undesired pyrolitic transformation of PMSSQ into SiO_2 occurs at temperatures higher than 600 °C.

The larger decrease of the film electron density in the case of the samples which initially contained some porogen (cf. Figure 8) clearly proves that the porogen was removed by calcination and that pores were created indeed.

The average electron density of the film which did not contain any porogen and which was cured at 420 °C could be determined to 405 nm^{-3}. From this value one may calculate the expected electron densities of a film composed of the same matrix material and cured at the same temperature but containing 10 or 20 vol % of voids filled with air (which have an essentially zero electron density). To judge the pore generation efficiency of the porogen used, these values are to be compared with those determined from the experimental data for the samples cured at 420 °C with initial porogen contents of 10 and 20%, respectively. In the case of 10% porosity, the calculated $\rho_{e,av}$(film) is 365 nm^{-3} as compared to the experimental value of 384 nm^{-3}. The corresponding values for 20% porosity are 324 and 370 nm^{-3}, respectively. In this calculation it was assumed, that the pore wall density of the matrix material equals the density of its nonporous analogue. This seems to be a good approximation, because the porosities under consideration are rather low. In both cases the experimental values of the film electron densities are considerably higher than those predicted for a pore generation efficiency of 100%. From the observed changes of the electron densities, the actual porosities may be estimated to 5% and 9% for the samples which originally contained 10% and 20% of porogen. One could thus consider that at the curing temperature of 420 °C the porogen might not be removed quantitatively from the film. On the other hand, TGA data of the PCL itself show that about 95% of the PCL decomposes at 420 °C. Due to the interaction of PCL and its decomposition products with the matrix material, however, it is likely that there exists a kinetic barrier for the diffusion of the decomposition products through the matrix. Part of the decomposition products could thus be trapped in the matrix. Furthermore it must be considered that in order to achieve a stable porous structure, it is essential that a sufficient stiffening of the matrix material occurs prior to the decomposition of the porogen. This might not be the case for the matrix/porogen system under consideration here. At the calcination temperature the pores that are created in the matrix could be shrinking to some degree due to a remaining mobility of the polymer chains during the calcination process. That would be an additional explanation for the experimentally observed porosities.

To date only one work appeared in the literature which reports the application of XR for the determination of porosities in PMSSQ/PCL hybrid systems.[6] There it was concluded that the porosities of the calcined films are close to the values that are expected for a complete replacement of the porogen by air-filled pores. Unfortunately, however, any information about experimental details is missing in that report and the XR data are not displayed. So we are not able to make a critical comparison between our work and the one mentioned above. In addition, the exact composition of the matrix material was not identical in both cases.

In fact, the presence of a thin surface skin layer with a slightly *increased* electron density, which we inferred from the low-frequency modulation of the reflectivity curve, is only one possible interpretation of the experimental data. It should be pointed out that the data may alternatively also be fitted by a model, which assumes a thin layer between the bulk of the film and the substrate, with an electron density in that interlayer being ca. 7% *lower* as compared to the bulk of the film. Even a model which incorporates both, such an interlayer and an additional surface skin layer, could describe the experimental data. This remaining ambiguity is due to the loss of phase information, which is inherent in any scattering method. Thus, a deduced electron density profile is usually not unique. On the other hand, for a given location of the thin layer, the phase of the corresponding oscillation unambiguously indicates whether the electron density of that layer is higher or lower as compared to the bulk of the film.

As the thin layer is present even in the films which are prepared without any porogen (evidenced by the observed oscillations shown in Figure 7), the origin of this layer cannot be due to an inhomogeneous distribution of the porogen or of the air-filled pores. This is also supported by the observation that the amplitude of the low-frequency oscillation is not significantly higher for the films where the porogen was removed by calcination as compared to the samples which still contained the porogen: If the inhomogeneity in the films was due to a nonuniform distribution of the porogen, the corresponding oscillation amplitude should markedly increase upon calcination due to the increased contrast. In consideration of this, the existence of a surface skin layer is most plausible: such a layer with a slightly increased electron density can be explained by the cooling process of the cured films, which proceeds from the film surface in the direction of the substrate. This could lead to a slightly increased film density in the surface region. Apart from this thin layer, the overall film structure was found to be homogeneous for all samples.

Conclusion

This is the first extensive work which demonstrated the possibility to use synchrotron X-ray reflectivity as a powerful tool to study the structure and density of both thin polyorganosilicate/porogen composite films as well as their nanoporous derivatives. Experimental procedures and a hierarchical fitting scheme of the reflectivity data

(29) Brinker, C. J.; Scherer, C. W. *Sol−Gel Science*, Academic: San Diego, 1990.

(30) Baney, R. H.; Itoh, M.; Sakakibara, A.; Suzuki, T. *Chem. Rev.* **1995**, *95*, 1409.

(31) Eisenberg, P.; Erra-Balsells, R.; Ishikawa, Y.; Lucas, J. C.; Mauri, A. N.; Nonami, H.; Riccardi, C. C.; Williams, R. J. *Macromolecules* **2000**, *33*, 1940.

were given for that purpose. In particular, careful measurements at smallest angles have proven to be a precise method to determine the average film electron density. This information can be used to judge the pore generation efficiency of a given matrix/porogen system. For the selected model system under consideration here, the porosity of the calcined films was less than expected for the case, that the porogen is completely removed at the calcination temperature and leaves behind air-filled pores. As a plausible explanation, we have discussed the possibility of a certain degree of shrinking of the generated pores. Making full use of high-intensity synchrotron X-ray radiation, the experimental data could be obtained in a very wide dynamic range over 9 orders of magnitude. This facilitated a precise determination of the total film thickness and film smoothness as well as the detection of possible inhomogeneities in the electron density profile. Evidence for overall homogeneous films with a thin surface skin layer, in which the electron density is slightly increased, could be given. It may be expected that in the future this experimental method will play an important role in the characterization and further development of porous spin-on glasses with superior properties.

Acknowledgment. This work was supported in part by the Korean Collaborative Project for Excellence in Basic System IC Technology (System IC 2010: 98-B4-C0-00-01-00-02) and by the Korea Science & Engineering Foundation (KOSEF) through the Center for Integrated Molecular Systems (CIMS). Financial support from the Korean Ministry of Education through the Brain Korea 21 Program is also gratefully acknowledged.

LA010451C